# Nonlinear electrostatic emittance compensation in kA, fs electron bunches

S. B. van der Geer and M. J. de Loos*
*Pulsar Physics, De Bongerd 23, 3762 XA Soest, The Netherlands*

J. I. M. Botman, O. J. Luiten, and M. J. van der Wiel
*Eindhoven University of Technology, Center for Plasma Physics and Beam Technology, P.O. Box 513, 5600 MB Eindhoven, The Netherlands*

(Received 2 October 2001; published 15 March 2002)

Nonlinear space-charge effects play an important role in emittance growth in the production of kA electron bunches with a bunch length much smaller than the bunch diameter. We propose a scheme employing the radial third-order component of an electrostatic acceleration field, to fully compensate the nonlinear space-charge effects. This results in minimal transverse root-mean-square emittance. The principle is demonstrated using our design simulations of a device for the production of high-quality, high-current, subpicosecond electron bunches using electrostatic acceleration in a 1 GV/m field. Simulations using the GPT code produce a bunch of 100 pC and 73 fs full width at half maximum pulse width, resulting in a peak current of about 1.2 kA at an energy of 2 MeV. The compensation scheme reduces the root-mean-square emittance by 34% to $0.4\pi$ mm mrad.

DOI: 10.1103/PhysRevE.65.046501 PACS number(s): 41.75.Lx, 07.05.Tp, 29.27.Bd, 41.85.Ne

## I. INTRODUCTION

Progress in accelerator physics is not only a matter of increasing the particle energy, but also depends critically on improvement of the particle beam brightness [1]. The brightness, a comprehensive measure for the beam quality, is the current density per unit solid angle and per unit relative particle energy spread. Obviously, beam brightness is an important quantity for collider experiments, as it determines the maximum current density, and thus the maximum event rate, that can be achieved by focusing the beam. Probably the most demanding application in this respect, however, is the x-ray self-amplified spontaneous-emission free electron laser (x-ray SASE FEL), which requires a 1 GeV electron beam with less than 1 % energy spread, with a current of 1 kA and a beam waist matching a diffraction limited x-ray beam [1,2].

In particular, the demands on the transverse degrees of freedom are severe. The transverse beam quality is expressed in terms of the normalized emittance, which is the area occupied by the beam in two-dimensional (2D) transverse $x-p_x$ (or $y-p_y$) phase space, in units [$\pi$ mm mrad]. It is a Lorentz-invariant measure for the focusability of the beam [3]. The x-ray SASE FEL requires a normalized emittance below 1 $\pi$ mm mrad.

Although the phase-space volume occupied by the beam is conserved during acceleration, nonlinear transverse forces may distort the shape of the distribution. This leads to an *apparent* increase of the transverse phase-space area, and thus effectively to undesirable emittance growth. For high-brightness applications it is, therefore, essential that nonlinear radial field components, which are caused by the space-charge self-field and by nonideal charged-particle optics, are either minimized or their effects compensated.

At present, the favorite tool for the initiation of high-brightness, low-emittance electron beams is the photocathode rf gun. In this device, a mode-locked laser is employed to photoexcite short (typically a few ps) and intense electron bunches from the inner surface of a high-field rf accelerator. These bunches do not yet have the current density required for SASE-FEL operation, since this would lead to intolerable space-charge-induced emittance growth. The bunches are, therefore, first accelerated to sufficiently high energies, which renders the radial space-charge forces harmless owing to relativistic cancellation of the Coulomb force by the Lorentz force. Subsequently, the bunches are compressed in a magnetic bend to the required 100 fs level. Unfortunately, however, magnetic compression gives rise to radiative collective effects, which spoil the emittance [4].

At Eindhoven University of Technology (TU/e) we have, therefore, adopted a different strategy. We aim at the production of 100 fs, 100 pC electron bunches with a normalized emittance below $1\pi$ mm mrad *without* the need for magnetic compression [5,6]. The key elements of our approach are: photoemission from a metal cathode by a fs laser assuming ''prompt'' emission and acceleration to the first 2 MeV by a 1 GV/m pulsed electrostatic field. In this way, the nonrelativistic part of the acceleration trajectory, in which the space-charge-induced emittance growth mainly occurs, is kept as short as possible. The ensuing 2-MeV bunch may then be accelerated to higher energies in a conventional rf accelerator without further deterioration. This approach is based on pioneer work at Brookhaven National Laboratories [7–9].

It is not it *a priori* clear that such a pulsed dc photocathode should yield superior results: first, if the bunch length is much smaller than the bunch radius, i.e., in a flat, disk-shaped geometry, the nonlinearity of the radial space-charge field is much more pronounced than in a ''cigar'' geometry; second, the necessarily small iris of the 1 GV/m electrostatic diode gives rise to highly nonlinear radial field components. In this paper, we show that the key to achieving a high beam quality is by having the detrimental effects due to these field

*Email address: gpt@pulsar.nl; http://www.pulsar.nl/gpt

 

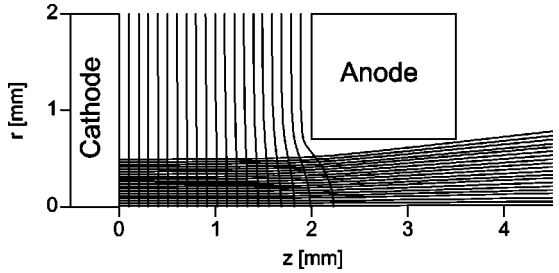


FIG. 1. Diode with potential lines and sample particle trajectories. Scales are in millimeters.

nonlinearities cancel each other. The characteristics of the bunches resulting from our simulations are well within the design specifications.

The nonlinear electrostatic emittance compensation scheme proposed in this paper is fundamentally different from the well-established compensation scheme based on slice-emittance alignment [10,11]. Whereas the former corrects for *distortion* of the shape of the beam in transverse phase space due to *nonlinear* radial space-charge forces, the latter corrects for *rotation* of the beam in transverse phase space due to *linear* radial space-charge forces. As they are essentially independent, a combination of the two compensation schemes may improve the beam quality of the pulsed dc photocathode even further.

The remainder of this paper is organized as follows. In Sec. II, the design of the TU/e pulsed dc photocathode is treated. In Sec. III, the simulation methods used are described and the results of the simulations presented. Section IV gives a detailed analysis of the mechanism of nonlinear electrostatic emittance compensation. Finally, Sec. V concludes this paper with a summary of the results and a brief outlook.

## II. PULSED DC PHOTOCATHODE

The TU/e pulsed dc photocathode consists of a flat copper cathode and an anode with a circular aperture, shown in Fig. 1. The cathode and anode are separated by 2 mm and the radius of the anode aperture is 0.7 mm. A 2 MV, 1 ns pulse generator, an upgrade of the device used in Ref. [8], supplies the 1 GV/m gradient across the 2 mm acceleration gap of this diode. This extreme field strength—almost an order of magnitude higher than in state-of-the-art rf accelerators—is possible because it is applied for only 1 ns, which is too short for electrical breakdown to occur.

Synchronization of the photoexcitation laser pulse with the 1 ns flat top of the 2 MV pulse is to be achieved by laser triggering of the spark gap in the high-voltage pulser. The photoexcitation laser pulse is injected on axis and has a 50 fs full-width-at-half-maximum (FWHM) Gaussian temporal profile and a 1 mm diameter flat-top (top-hat) radial profile. The choice of an initial beam radius of 0.5 mm is a compromise between bunch lengthening due to space charge at small initial radius and increase of the thermal (or initial) emittance at large initial radius. The design simulation parameters are listed in Table I.

The aperture in the anode acts as a negative lens and is kept as small as possible to prevent the field from leaking out of the gun and thereby lowering the acceleration field. As a result, the outer radial part of the bunch passes through the anode at a very small distance from the inner surface of the aperture. Since deviations from ideal lens behavior are maximal at the electrode surface, it is unavoidable that the bunch is subjected to highly nonlinear radial fields.

TABLE I. Simulation parameters.

| | |
|---|---|
| Accelerating voltage | 2 MV |
| Gap length | 2.0 mm |
| Bunch charge | 100 pC |
| Temporal profile laser pulse | Gaussian, 50 fs FWHM |
| Radial profile laser pulse | Flat top, 0.5 mm radius |
| Anode aperture radius | 0.7 mm |
| Initial particle energy | 0.4 eV |
| Initial velocity distribution | Isotropic |

We find that the beam has a laminar flow in the diode. Throughout the entire acceleration process the bunch length is much smaller than the bunch radius, i.e., the bunch maintains a flat disk shape.

Eventually, the diode will be followed by a $2\frac{1}{2}$-cell rf cavity to increase the bunch energy to 10 MeV. The matching of the electrostatic diode to the $2\frac{1}{2}$-cell rf cavity and the characteristics of the bunch at 10 MeV will be the subject of a forthcoming paper.

## III. SIMULATIONS

Simulations for the design of the diode were performed using the general particle tracer (GPT) simulation package [12,13]. GPT is a commercially available time-domain 3D particle tracking code developed for the design of accelerators and beam lines. The differential equations for the particle trajectories are solved using a fifth-order embedded Runge-Kutta method.

The 2D space-charge model of GPT was used, instead of the standard 3D point-to-point model, because the system is cylindrically symmetric. For the simulations presented in this paper, GPT was used in combination with the POISSON [14] set of codes to calculate the field map of the diode. The effects of image charges in the cathode and wakefields in the anode are not included in the simulations. A straightforward estimate shows that the field associated with image charges at the cathode surface is negligible compared to the 1 GV/m acceleration field.

### A. Simulation results: Longitudinal phase space

Figure 2 shows the longitudinal phase-space characteristics of the resulting 2 MeV bunch at a position $z=4.5$ mm, i.e., 1 mm after the exit of the diode. In Fig. 2(a), the bunch distribution in $z-E$ longitudinal phase space is plotted. After acceleration to 2 MeV the initially monoenergetic 100 pC 50 fs bunch attains a 30 keV FWHM energy spread and a FWHM bunch length of 73 fs. We will now discuss the 2 MeV longitudinal phase-space distribution in more detail.

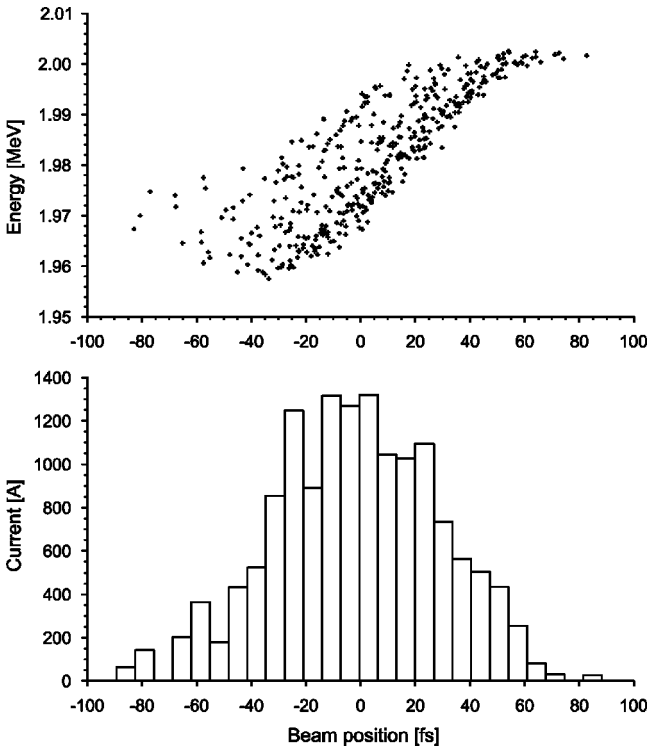


FIG. 2. (a) The bunch distribution in $z-E$ longitudinal phase space at a distance of $z=4.5$ mm from the cathode surface. (b) Beam current as a function of longitudinal position at $z=4.5$ mm.

The spread in longitudinal particle velocities due to the 30 keV energy spread is the main cause of the increase of the FWHM bunch length from 50 fs to 73 fs. The energy spread is due to axial space-charge forces, which give the electrons in the front part of the bunch an additional boost, while slowing down the electrons in the back. This manifests itself as a counterclockwise rotation of the (initially flat-line) particle distribution in $z-E$ phase space, leading to the positive energy-position correlation of Fig. 2(a). The axial space-charge force depends linearly on $z$ in the center of the bunch, which is reflected in the linear energy-position correlation of the central part. At the bunch extremities, however, the axial space-charge force becomes increasingly nonlinear as it drops off to zero. As a result, the rotation in $z-E$ phase space of the front and the back of the bunch is slower than the rotation of the central part, giving rise to an *S*-shape distribution.

In addition to the space-charge-induced energy spread, there is a second bunch-lengthening mechanism, associated with the particular field geometry of the diode. As the diode acts as a negative lens, the initially flat, disk-shaped bunch acquires a curved, hollow shape with the central part of the disk somewhat ahead of the outer radial part. After averaging over radial position this leads effectively to an increase of the bunch length. It is, however, only a minor contribution: by ''switching off'' the space-charge forces in the simulations we find that this geometric effect increases the FWHM bunch length merely from 50 fs to 58 fs. The positive curvature of the bunch at $z=4.5$ mm is reflected in the diffuse, asymmetric broadening of the longitudinal phase-space distribution in Fig. 2(a): the densely populated *S*-shaped area corresponds to the central part of the disk, while the diffuse cloud lagging behind corresponds to the off-axis part.

Since axial space-charge forces are relativistically suppressed at higher energies, they mainly affect the bunch at its initiation. Further acceleration will, therefore, not lead to any significant space-charge-induced increase of the 30 keV FWHM energy spread. The time-varying rf fields that will be employed for further acceleration will not lead to any significant increase of the energy spread either, because the bunch is extremely short compared to an *S*-band rf period. We therefore expect that the bunch will easily meet the relative-energy-spread requirements at higher energies.

In Fig. 2(b), the beam current at $z=4.5$ mm is plotted as a function of longitudinal position in the bunch. The peak current is well over 1.2 kA, well within SASE FEL specifications.

### B. Simulation results: Transverse phase space

The normalized root-mean-square (RMS) transverse emittance in the $x$ direction is calculated in [$\pi$ mm mrad] by

$$\varepsilon_{x,RMS}=\sqrt{\langle x^2\rangle\langle\gamma^2\beta_x^2\rangle-\langle x\gamma\beta_x\rangle^2}, \tag{1}$$

where $\gamma\equiv(1-\beta^2)^{-1/2}$ is the Lorentz factor, $\beta\equiv v/c$ the normalized particle velocity, $\beta_x$ the normalized velocity in the $x$ direction, and $\langle\ \rangle$ denotes the weighted average over all particles.

Applying Eq. (1) to the initial beam parameters listed in Table I, a thermal emittance of $0.23\pi$ mm mrad is obtained. This is a conservative estimate of the real initial emittance, since both the isotropic initial velocity distribution and the monoenergetic 0.4 eV initial particle energy distribution are ''worst-case'' assumptions. The simulations based on this initial condition should, therefore, give an upper-bound estimate of the emittance that can be achieved.

From the simulations, we find that after acceleration to 2 MeV the bunch at $z=4.5$ mm is characterized by a normalized RMS transverse emittance of about $0.4\pi$ mm mrad, which is well within specifications. This result is particularly good considering the fact that the bunch is subjected to large nonlinear radial forces.

To illustrate how nonlinear radial forces affect the bunch, the distribution in $r-p_r$ transverse phase space is plotted in Fig. 3 at the bunch position $z=0.85$ mm. At $z=0.85$ mm the accelerating field is still highly uniform and the radial forces that have been acting on the bunch are mainly due to space charge. Also shown is the initial $z=0$ transverse phase-space distribution, indicated by the horizontal rectangular shape.

The radial space-charge forces are zero at the axis and increase with radial distance from the axis, blowing up the bunch in the transverse direction. The larger the radial distance from the axis, the larger the radial force and thus larger the additional radial momentum $p_r\equiv mc\gamma\beta_r$ that is acquired. If the radial force is proportional to $r$, as is the case in a uniform, continuous beam, this would result in a counterclockwise rotation of the distribution in $r-p_r$ transverse

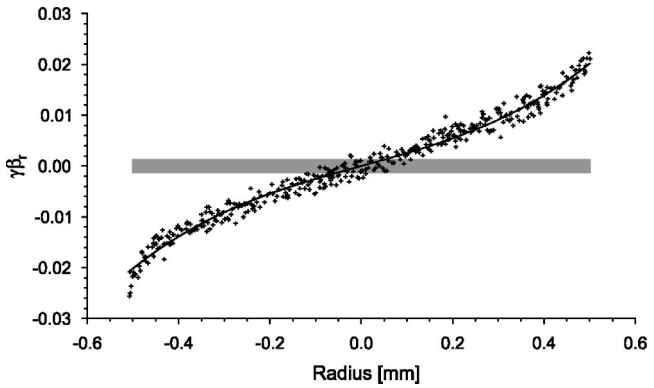


FIG. 3. The bunch distribution in $r-p_r$ transverse phase space at a distance of $z=0.85$ mm from the cathode surface. The *S*-like distortion of the shape of the distribution is mainly due to nonlinear radial space-charge forces immediately after initiation of the bunch. The solid curve is a third-order polynomial fit. The initial $z=0$ transverse phase-space distribution is indicated by the horizontal rectangular shape.

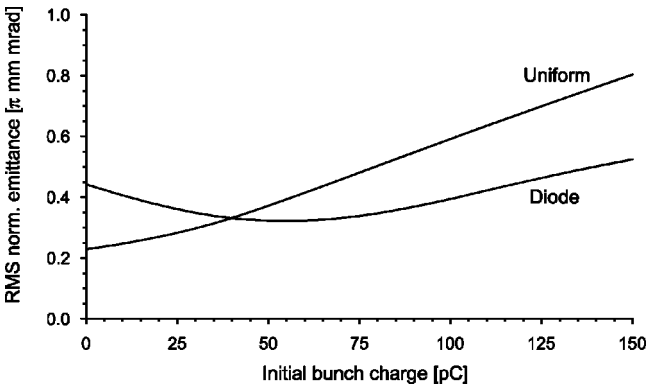


FIG. 4. Normalized transverse emittance as function of bunch charge at a distance of $z=4.5$ mm from the cathode surface, for both a uniform field configuration and the realistic diode geometry.

phase space. Since in this process the phase-space surface area is conserved, the normalized transverse emittance is not affected. Figure 3 shows that this is approximately the case for the central part of the bunch. Near the outer radius of the bunch, however, nonlinear radial forces become increasingly important, leading to an *S*-like distortion of the shape of the distribution.

The distorted distribution effectively occupies a larger area in transverse phase space, which is reflected in the increased value of the RMS normalized emittance: $\varepsilon_{RMS}=0.4\pi$ mm mrad at $z=0.85$ mm. Surprisingly, this is equal to the final value of the bunch emittance at $z=4.5$ mm. Since it is highly unlikely that the bunch does not suffer any further emittance growth in between, this result suggests that some subtle emittance compensation process is involved in the remainder of the acceleration.

To get a clear view of the processes involved, it is instructive to separate space-charge effects from the effects of the nonideal accelerating field. The simulations have, therefore, been performed as a function of bunch charge both in the realistic diode field and in a hypothetical uniform electrostatic acceleration field without any radial components. In Fig. 4, the RMS normalized transverse emittance at $z=4.5$ mm, i.e., the emittance after acceleration to 2 MeV, is plotted as a function of initial bunch charge for both field geometries. The hypothetical, uniform acceleration field gives rise to a monotonous increase of the final RMS emittance as a function of initial bunch charge, as space charge is the only mechanism involved. Because both systems have a peak gradient of 1 GV/m and accelerate to 2 MeV, one would expect the final RMS emittance to be worse in the case of the realistic diode field due to the nonlinear transverse fields caused by the hole in the anode. Surprisingly, this is only true for *small* bunch charges: it turns out that for charges larger than 40 pC the RMS emittance results are significantly better for the realistic diode field than for the idealized uniform field, as is shown in Fig. 4. As will be explained in more detail in the next section, the field curvature due to the anode geometry effectively compensates the nonlinear part of the space-charge field, thus significantly reducing RMS emittance growth.

## IV. NONLINEAR ELECTROSTATIC EMITTANCE COMPENSATION

### A. Radial space-charge field

The dynamics of flat, disk-shaped bunches is quite different from the dynamics of elongated cigar-shaped bunches, because the radial component of the space-charge self-field as function of radial position *r* in flat bunches is generally far from linear. To illustrate this effect, the radial component $E_r$ of the space-charge field in the median plane of a short and a relatively long bunch is plotted as a function of *r* in Fig. 5.

Both bunches have a 1 mm diameter uniform radial density profile and a Gaussian axial density profile, in accordance with our initial conditions. For both cases, the radial field $E_r$ is normalized to its value at the outer radius of the bunch ($r=0.5$ mm). The FWHM length of the short bunch in its rest frame is $100\,\mu$m, corresponding to a FWHM length of 67 fs at 2 MeV, i.e., approximately the geometry of the bunch emerging from the diode. The long bunch has

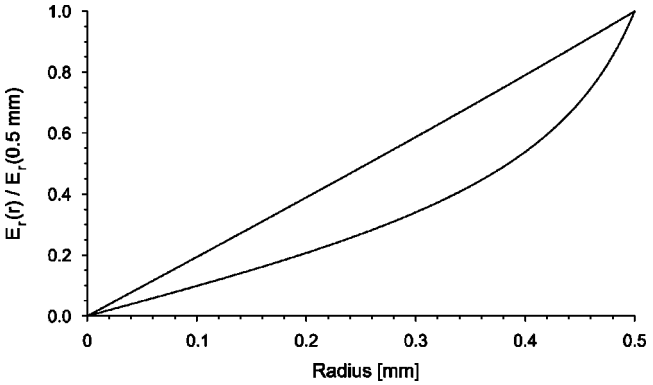


FIG. 5. Radial component of the electric self-field in the median plane of a short and a long bunch, both with a 1 mm diameter rectangular radial density profile and Gaussian axial density profile.

FWHM length in its rest frame of 2 mm, corresponding to a FWHM length of 1.3 ps at 2 MeV.

The radial self-field of the long bunch is nearly indistinguishable from the radial field in a uniform, continuous beam (infinitely long bunch), i.e., $E_r$ proportional to $r$ all the way up to the outer radius of the bunch. The radial field in the short bunch, however, has a strong, positive nonlinear component. The fact that this nonlinearity has a positive sign, i.e., the curve in Fig. 5 bends *upwards*, can be explained by considering a short bunch and a long bunch with the same space charge density: The radial field in the median plane of a short bunch is smaller than the radial field of a long bunch, simply because there is less charge contributing to the field. The radial field in a point near the outer radius of the bunch is mainly due to the charges close to this point. The radial field in a point near the center of the bunch, however, is determined by charges near the outer radius, i.e., at a large distance from this point, because the contributions from charges nearby cancel each other. Decreasing the bunch length, while maintaining the bunch radius and the space charge density will, therefore, decrease the radial field near the center more strongly than the radial field near the outer radius, giving rise to the behavior depicted in Fig. 5.

The fact that the increase of the radial space-charge forces with radial distance is stronger than linear is reflected in the direction of the *S*-shape distortion in transverse phase space (upward on the right, and downward on the left), as shown in Fig. 3. A different radial beam density, for example, created by using a truncated Gaussian radial laser profile on the photocathode, can reduce this effect [15].

### B. Total radial field

The radial electrostatic field of the diode has a large nonlinear component near the anode opening. The field is well described by a third-order polynomial of the form $E_r = E_{r,1} r + E_{r,3} r^3$, where $r$ is the radial position and the coefficients $E_{r,1}(z)$ and $E_{r,3}(z)$ are both functions of the longitudinal position $z$. The third-order coefficient $E_{r,3}$ gives rise to spherical aberration of the diode lens.

The total electric field acting on the particle beam is the sum of the external field *and* the space-charge field. The third-order coefficient, $E_{r,3}$, of the radial component of the total field is plotted as a function of $z$ in Fig. 6(a) for our 100 pC bunch, both for the hypothetical uniform acceleration field of 1 GV/m and for the realistic diode field. In the uniform case, space charge is the only mechanism causing third-order terms. The third order coefficient $E_{r,3}$ increases monotonously during the acceleration ($0 \leqslant z \leqslant 2$ mm) and decreases slowly again as the bunch lengthens in the free drift space ($z \geqslant 2$ mm). In the realistic diode geometry near the cathode, $E_{r,3}$ behaves similarly because there the external field is approximately uniform. But near the anode ($z = 2$ mm), where the beam has already been accelerated to well over 1 MeV, the third-order term is dominated by the external field.

### C. Evolution in transverse phase space

The evolution of the particle distribution of the bunch in transverse phase space ($\gamma\beta_r \equiv p_r/mc$ vs $r$) is governed by

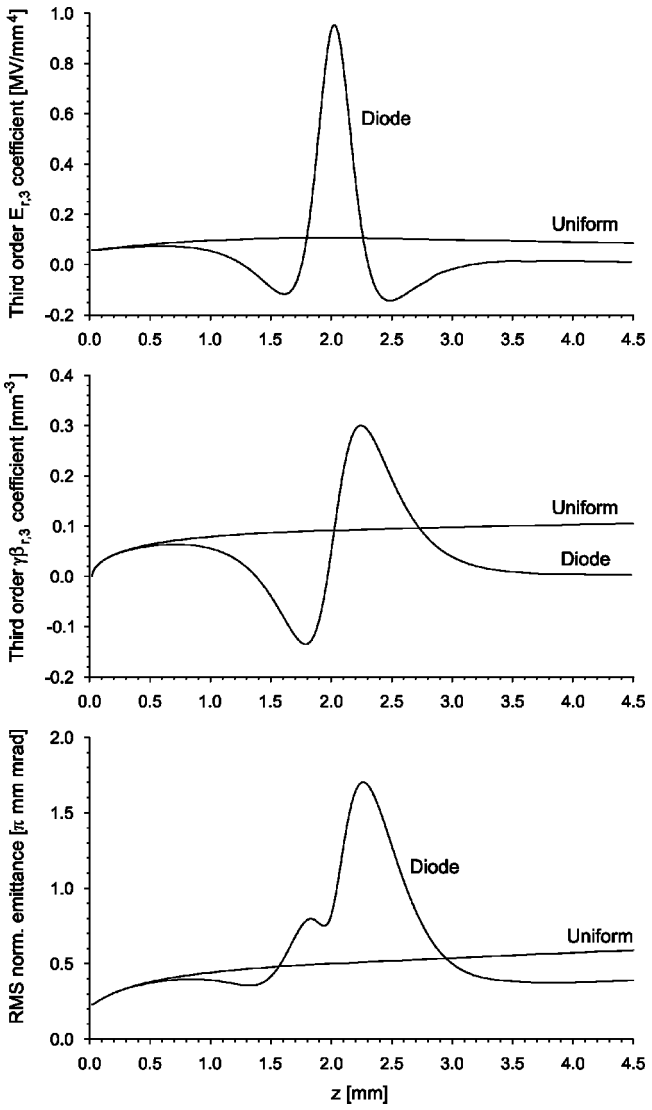


FIG. 6. (a) Third-order coefficient $E_{r,3}$ of the radial component of the total electric field as a function of $z$ for a bunch charge of 100 pC, for both the hypothetical uniform field and the realistic diode field. (b) Corresponding third-order coefficient $\gamma\beta_{r,3}$ of the polynomial fit to the bunch shape in transverse phase space as a function of $z$. (c) Corresponding normalized RMS emittance as a function of $z$.

$E_r$. We describe the shape of this distribution analogously to the radial field component by fitting it with a third-order polynomial of the form $\gamma\beta_r = \gamma\beta_{r,1} r + \gamma\beta_{r,3} r^3$, where the coefficients $\gamma\beta_{r,1}(z)$ and $\gamma\beta_{r,3}(z)$ are both functions of the longitudinal position $z$. An example of such a fit is shown in Fig. 3. Changes in the linear coefficient $\gamma\beta_{r,1}$ describe linear transformations in transverse phase space, like rotations, which have no effect on the RMS emittance. The third-order coefficient $\gamma\beta_{r,3}$, however, describes an *S*-shape distortion in transverse phase space. This results in RMS emittance growth, although the actual area in phase space is preserved [3].

The third-order component of the shape of the transverse phase-space distribution, $\gamma\beta_{r,3}$, is strongly related to the integrated third-order component in the transverse electric

field, $E_{r,3}$. In a uniform field $E_{r,3}$ is always positive, resulting in a steady increase of $\gamma\beta_{r,3}$, as shown in Fig. 6(b). This in turn results in the steady increase in RMS emittance shown in Fig. 6(c).

In the realistic diode geometry, the particle distribution in transverse phase space is also affected by the strong nonlinearities of the external field near the anode aperture. The geometry of the diode is chosen such that these nonlinearities fully compensate the nonlinear space-charge effects, resulting in a zero $\gamma\beta_{r,3}$ component at the exit of the diode. Therefore, the lowest possible RMS emittance contribution is achieved, a 34% improvement over the case of a uniform field.

We will now discuss the behavior of the RMS normalized emittance of the bunch during the acceleration process in the realistic diode geometry in more detail. Initially, for $z \leqslant 0.5$ mm the emittance growth follows the behavior of the uniform field geometry, as it is governed by space-charge forces. For $z \geqslant 0.5$ mm, however, the negative third-order coefficient of the external field starts to compensate the space-charge-induced emittance growth, resulting in a local maximum of $\varepsilon_{RMS}$ at $z=0.85$ mm. The negative third-order coefficient of the external field is sufficiently strong to change the sign of $\gamma\beta_{r,3}$, i.e., the *S* shape of Fig. 3 flips into the opposite orientation. As $\gamma\beta_{r,3}$ goes through zero, $\varepsilon_{RMS}$ goes through a minimum at $z=1.35$ mm. The external field overcompensates the space-charge effects, however, leading to a local maximum in the RMS emittance at $z=1.8$ mm. This is the position where the integrated effect of the negative $E_{r,3}$ is maximal, i.e., approximately the position where $E_{r,3}$ changes sign. The positive third-order coefficient of the external field subsequently slightly compensates for the previous overcompensation, resulting in a local minimum in $\varepsilon_{RMS}$ at $z=1.95$ mm. The positive third-order coefficient of the external field then pushes the RMS emittance to an absolute maximum at $z=2.25$ mm. Finally the third-order coefficient of the external field changes sign again, restoring the RMS emittance practically to the value it had before the external nonlinear fields became active.

The overall effect of the external nonlinear fields is a compensation of an *S*-shape distortion due to space-charge fields as depicted in Fig. 3. This means that in absence of space-charge forces the spherical aberration of the diode lens would give rise to an *S*-shape distortion with the opposite orientation. This seems to be in contradiction with Scherzers theorem [3,16], which states that spherical aberration of charged particle lenses is always of the same sign, giving rise to an *S*-shape distortion with an orientation as depicted in Fig. 3. Interestingly, Scherzers theorem does not hold for our case, since we are dealing with a so-called cathode lens, in which the usual paraxial equation does not apply (see Chap. 18 of Ref. [16]).

## V. CONCLUSION AND OUTLOOK

The already low emittance achievable in the pulsed dc photocathode can even further be improved by employing nonlinear electrostatic emittance compensation. Using this method 100 pC, 73 fs FWHM bunches can be produced at 2 MeV with a normalized emittance of $0.4\pi$ mm mrad. The diode setup results in an emittance improvement of 34% for short bunches when compared to a uniform acceleration field by completely compensating the third-order effect of the space charge.

The characteristics of the accelerated bunch at 2 MeV are well within the design specifications, and therefore compatible with x-ray SASE FEL requirements. Because of the extremely high gradient and because no external focusing is needed, this device could be much better suited for ultrashort bunch generation than a conventional photocathode rf gun. In a forthcoming paper, we will show that this bunch can be accelerated in a booster without too much deterioration. The 30 keV FWHM energy spread will not increase significantly in the rf booster because the bunch is extremely short compared to an *S*-band rf period. Furthermore, a compensation scheme based on slice-emittance alignment will be incorporated to further improve the emittance.

## ACKNOWLEDGMENT

The authors would like to thank Luca Serafini for his interest in this project and his stimulating comments.

[1] M. J. van der Wiel, in *Proceedings of the Second ICFA Future Accelerator Workshop on the Physics of High-Brightness Beams, Los Angeles, 1999*, edited by J. Rosenzweig and L. Serafini (World Scientific, Singapore, 2000).

[2] J. Andruskov *et al.*, Phys. Rev. Lett. **85**, 3825 (2000).

[3] S. Humphries, *Charged Particle Beams* (Wiley, New York, 1990).

[4] B. Carlsten and T. Raubenheimer, Phys. Rev. E **51**, 1453 (1995).

[5] M. J. de Loos, S. B. van der Geer, J. I. M. Botman, O. J. Luiten, and M. J. van der Wiel, in *Proceedings of the IEEE Particle Accelerator Conference, 1999*, edited by A. Luccio and W. MacKay (IEEE, Piscataway, NJ, 1999) p. 3266.

[6] F. B. Kiewiet, O. J. Luiten, G. J. H. Brussaard, J. I. M. Botman, and M. J. van der Wiel, in *Proceedings of the European Particle Accelerator Conference, Vienna, Austria, 2000*, edited by J.-L. Laclare *et al.* (Austrian Academy of Sciences Press, Vienna, 2000), p. 1660.

[7] T. Srinivasan-Rao and J. Smedley, in *Advanced Accelerator Concepts*, edited by Swapan Chattopadhayay, Julie McCullough, and Per Dahl, AIP Conf. Proc. 398 (AIP, Woodbury, NY, 1997), p. 730.

[8] K. Batchelor *et al.*, in *Proceedings of the European Particle Accelerator Conference, Stockholm, Sweden, 1998*, edited by S. Meyers *et al.* (IOP, London, 1998), p. 791.

[9] T. Srinivasan-Rao, J. Schill, I. Ben-Zvi, K. Batchelor, J. P. Farrell, J. Smedley, X. E. Lin, and A. Odian, in *Proceedings of the IEEE Particle Accelerator Conference, New York, 1999*,

edited by A. Luccio and W. MacKay (IEEE, Piscataway, NJ, 1999), p. 75.

[10] B. Carlsten, Nucl. Instrum. Methods Phys. Res. A **285**, 313 (1989).

[11] L. Serafini and J. B. Rosenzweig, Phys. Rev. E **55**, 7565 (1997).

[12] S. B. van der Geer and M. J. de Loos, in *Proceedings of the European Particle Accelerator Conference, Stockholm, Sweden, 1998*, edited by S. Myers *et al.* (IOP, London, 1998), p. 1245.

[13] S. B. van der Geer and M. J. de Loos, Pulsar Physics Report No. 2.52 (unpublished).

[14] J. H. Billen and L. M. Young, Los Alamos National Laboratory Report No. LA-UR-96-1834, 1998 (unpublished).

[15] L. Serafini, in *Advanced Accelerator Concepts* edited by Jonathan S. Wurtele, AIP Conf. Proc. 279 (AIP, New York, 1993), p. 645.

[16] P. W. Hawkes and E. Kasper, *Principles of Electron Optics* (Academic Press, New York, 1989).